

²⁶ Becker, J. V. and Korycinski, P. F., "Heat Transfer and Pressure Distribution at Mach Number of 6.8 on Bodies with Conical Flares and Extensive Flow Separation," TN D-1260, April 1962, NASA.

²⁷ Goldberg, T. J., "Turbulent Separation Associated with Axisymmetric Flared Bodies," *Journal of Spacecraft and Rockets*, Vol. 4, No. 11, Nov. 1967, pp. 1551-1553.

²⁸ Henderson, J. H., "Jet Effects on Base Pressures of Cylindrical and Flared Afterbodies at Free-Stream Mach Numbers of 1.65, 1.82 and 2.21," ARGMA TR 1G3R, June 1960; U.S. Army Ordnance Missile Command, Redstone Arsenal, Ala., classification change to unclassified March 21, 1961.

A Method for More Reproducible Burning Rate Determination

W. T. BROOKS*

Rocketdyne/North American Rockwell Corporation,
McGregor, Texas

Nomenclature

A_b	= burning surface area
A_t	= nozzle throat area
a	= constant in burning rate equation
c^*	= characteristic exhaust velocity
g_c	= gravitational conversion constant
n	= pressure exponent
P	= pressure
r, r'	= burning rate, Eqs. (1) and (4), respectively
t_b	= burning time
W_p, w	= propellant weight and web thickness, respectively
ρ_p	= propellant density
σ, σ'	= standard deviations for r and r' , respectively

Introduction

CONVENTIONAL methods for calculating burning rate from a solid propellant motor test firing rely on measured values of burning duration and propellant web distance. A simple manual method is given here with supporting data which provides in many cases a more reproducible burning rate for sliverless motors. It is relatively insensitive to selection of the aft tangent point, and has particular application to burning rate reduction from laboratory scale motors.

Discussion

Burning rate is typically defined by

$$r = w/t_b \quad (1)$$

The web (w) is a straightforward measure. Burning time (t_b) is measured from the pressure- or thrust-time record. Customarily, it is defined to be the interval ending when pressure begins to drop rapidly before going into tailoff. Mathematically, this occurs when $d^3p/dt^3 = 0$. Graphically, it may be determined by the widely used method of bisecting the angle between tangents to the pressure-time [$P(t)$] curve on either side of the point where the third derivative vanishes. In either event, impulse delivered beyond this point is variable, and the magnitude of measured burning time as well as tailoff impulse significantly influences the calculated burning rate.

The method considers burning rate from the simplified pressure equation

$$\bar{P} = \bar{A}_b \rho_p c^* r / g_c A_t \quad (2)$$

It should be noted that average pressure from the $P(t)$ curve may not be identical to \bar{P} in Eq. (2) for non-neutral traces.¹ The same can be said for a comparison of the burning rates (r) given in Eqs. (1) and (2).² These effects are small, however, and the $P(t)$ traces considered here are reasonably neutral burning.

If the values of c^* and ρ_p in Eq. (2) are replaced by

$$c^* = g_c A_t \int P dt / W_p \text{ and } \rho_p = W_p / \bar{A}_b w \quad (3)$$

burning rate becomes

$$r' = w \bar{P} / \int P dt \quad (4)$$

where the integrals are taken over the total duration.

Equation (4) is equivalent to the ratio of web and time, where

$$t = \int P dt / \bar{P} \quad (5)$$

This was defined as effective time in Ref. 3. Average pressure (\bar{P}) is taken to be the average over burning time ending at the aft tangent point. Although assessment of the aft tangent time is necessary in both Eqs. (1) and (4), the magnitude of \bar{P} in Eq. (4) is much less sensitive than t_b in Eq. (1) to the procedure for determining the end of burning time.

Considering a typical subscale test motor with a neutral internal burning tube, Eq. (1) gives the most accurate results from tests yielding the least amount of impulse in the tailoff. Influence of this variable (tailoff impulse) on Eq. (1) should be recognized in assessing the accuracy of the method as well as the burning rate where sliverless grains are used. For example, two aft tangent point selections on the $P(t)$ trace from two independent analyses, one at t_1 and one at $t_1 + \Delta t$, will define burning rates from Eq. (1) which differ by the fraction $(t_1 + \Delta t)/t_1$. Average pressures in Eq. (4) over the two intervals differ by an amount much less than the same fraction. Therefore, the burning rate determined by Eq. (4) is better defined than the burning rate by Eq. (1). In the case where no tailoff exists, Eqs. (4) and (1) are the same. Otherwise, $r' < r$.

Data and Results

The method has been evaluated over a range of burning rate from 0.3 to 0.8 in./sec in a 2-in. motor with carboxy-terminated polybutadiene (CTPB) aluminized propellant. The 2-in. motor has an internal burning tube with outer diameter

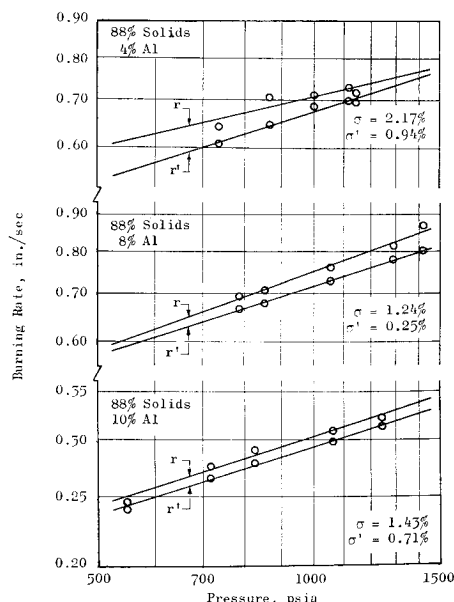


Fig. 1 Comparison of burning rate methods for 3 propellants.

of 2.37 in., inner diameter of 1.37 in., and length of 4.20 in., with ends unrestricted. The motors were conditioned to 77°F for firing, and five from a mix were fired for burning rate determination. Typical data are presented for these propellants in Fig. 1. The least squares lines were derived using de Saint Roberts burning rate law $r = aP^n$ that, although not universally true, suitably applies to these and other propellants.

The notable benefit derived from this method is typified by the lower standard deviation for r' indicated in Fig. 1. Generally, significant deviation of r from the line reflects variation in tailoff impulse. These show that r' is relatively independent of tailoff characteristics, as well as data reduction techniques for determining the aft tangent point. Therefore, Eq. (4) is likely to produce consistently a more reproducible burning rate.

A reasonable correlation was obtained between r' and full-scale motor burning rate. Typically, r' is 2-4% below corresponding full-scale motor burning rate. In particular applications, the 4 and 10% Al propellants demonstrated 2-in. r' 2 and 3% lower, respectively, than r in the full-scale motor. A burning rate of 0.749 in./sec at 1000 psia was derived from a full-scale motor firing with the mix of 8% Al propellant, in which $r' = 0.716$ in./sec. In reconciling this difference, it is recognized that average burning rate, derived by relating web to burning time and average pressure, reflects in particular the degree of augmentation from erosive burning as well as induces a slight error previously noted.²

References

- ¹ Rossini, R. A., Billheimer, J. S., and Threewit, T. R., "Configuration Efficiency: A New Measure of Ballistic Quality for Grain Design," *ARS Journal*, Vol. 31, No. 12, Dec. 1961, pp. 1761-1764.
- ² Brock, F. H., "Average Burning Rate, Average Pressure Relationships in Solid Rockets," *Journal of Spacecraft and Rockets*, Vol. 3, No. 12, Dec. 1966, pp. 1802-1803.
- ³ Bartley, C. D., "Application of Simplified Method for Determining the Internal-Ballistic Characteristics of Solid Propellants," CIT/JPL-PR-20-153, Nov. 1951, Jet Propulsion Laboratory, California Institute of Technology, Pasadena, Calif.

Investigation of High Mass Ratio, Multiple-Nozzle, Air-Ejector Systems

W. A. WRIGHT*

ARO, Inc., Tullahoma, Tenn.

AND

F. SHAHROKHI†

University of Tennessee Space Institute,
Tullahoma, Tenn.

LARGE, low-speed ground-testing facilities are of current interest, particularly for testing V/STOL aircraft. Motor-driven propeller systems for pumping full-scale ground test tunnels are very expensive, and elimination of this requirement in open circuit tunnels would effect considerable capital savings. One concept for this type of facility is to use a large

Presented as Paper 70-579 at the AIAA 5th Aerodynamic Testing Conference, Tullahoma, Tenn., May 18-20, 1970; submitted May 25, 1970; revision received August 13, 1970. The research herein was sponsored by Headquarters AEDC, Arnold Air Force Station, Tenn., Contract AF 40(600)-1200 with ARO, Inc.

* Project Engineer.

† Associate Professor. Associate Fellow AIAA.

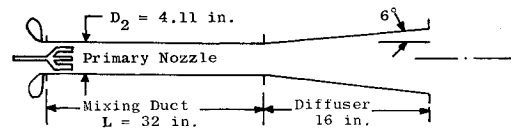


Fig. 1 Ejector configuration components, and dimensions used for the data presented herein.

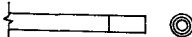
number of air ejectors in parallel to pull air through the test section. By varying the operation of various groups of these ejectors, tunnel operation presumably could be made very flexible.

There have been many studies¹⁻⁴ of jet pumps directed toward understanding of the flow phenomena and generation of a unified theory to explain the physical behavior within the flowfields. Fabri and Paulon¹ conducted an intensive investigation of the interaction between primary and secondary streams of ejector systems. Practically all of the studies considered the jet pump in the role of a pressure pumping device capable of producing a large pressure ratio from inlet to outlet under conditions favorable to this method of operation. Chisholm⁵ entered the region of high secondary/primary mass flow ratios (that would be of interest here) in an investigation of thrust- and mass-augmentation using an air ejector; however, available data for high mass ratio pumping was meager. The present investigation was made to generate some data and define ejector operating characteristics in this region.


It was believed that use of multiple primary nozzles in each ejector would enhance performance and/or permit a reduction in ejector length. Therefore, data were obtained using multinozzle systems arranged in symmetric configurations intended to divide equally the mixing duct area, as well as single-nozzle configurations (Fig. 1). Secondary air at atmospheric ambient conditions was pumped through the ejector by free turbulent mixing with the higher energy driving jets in a momentum exchange process with the near-ambient total-temperature primary air taken from a shop air line. Primary driving air total pressure was varied systematically over a pressure ratio range (primary/secondary) from 1.9/1 to 8/1. Area ratios (secondary/primary) ranged from approximately 80/1 to 650/1. The mixed stream was discharged to the atmosphere in all cases.

The basic equations employed in the analysis were derived using the von Kármán integral method, wherein the stream velocity profile is prescribed. Mixing of the primary and secondary streams was assumed to occur according to the Prandtl theories concerning mixing length for turbulent shear and the eddy viscosity model, following Peters's^{6,7} theoretical development. The modified analysis included a wall correction for boundary-layer displacement thickness δ^* by applying a factor to the duct wall radius as follows: $r_w = C_1 + C_2x$, where C_2 represents the displacement thickness ($-d\delta^*/dx$). This analysis considered the back-pressure-dependent mode of operation, wherein the back pressure P_b was always high enough to preserve subsonic secondary flow throughout the length of the ejector, and the exit pressure was identical to the back pressure. Geometric "equivalency" factors were applied to the multinozzle configurations on the basis of equal

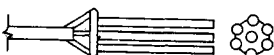
Primary Nozzle Group:



Type I	$(L/D)_{eq}$	Total A_p^* in. ²	Figs.
(1 Noz.)	7.8	0.0774	3,5



Type II	$(L/D)_{eq}$	Total A_p^* in. ²	Figs.
(3 Noz.)	4.5	0.0693	3,5
		0.0202	4



Type III	$(L/D)_{eq}$	Total A_p^* in. ²	Figs.
(7 Noz.)	2.9	0.0653	3,5

Fig. 2 Details of ejector inlet and primary nozzle configurations used for data reported herein.